THE JOURNAL OF PHYSICAL CHEMISTRY A

Article

pubs.acs.org/JPCA

Angle-Dependent Ionization of Hydrides AH_n Calculated by Time-Dependent Configuration Interaction with an Absorbing Potential

Pascal Krause and H. Bernhard Schlegel*

Wayne State University, Department of Chemistry, Detroit, Michigan, United States

Supporting Information

ABSTRACT: The angle dependence of strong-field ionization was studied for a set of second period hydrides (BH_3, CH_4, NH_3, H_2O, and HF) and third period hydrides (AlH_3, SiH_4, PH_3, H_2S, and HCl). Time-dependent configuration interaction with a complex absorbing potential was used to model ionization by a seven cycle 800 nm cosine squared pulse. The ionization yields were calculated as a function of the laser polarization and plotted as three-dimensional surfaces. The general shapes of angular dependence can be understood in terms of ionization from the highest occupied orbitals. Variations in the shapes with laser intensity indicate that ionization occurs not just from the highest occupied orbitals, but also from lower-lying orbitals. These deductions are supported by variations in the population analysis with the intensity of the laser field and the direction of polarization.

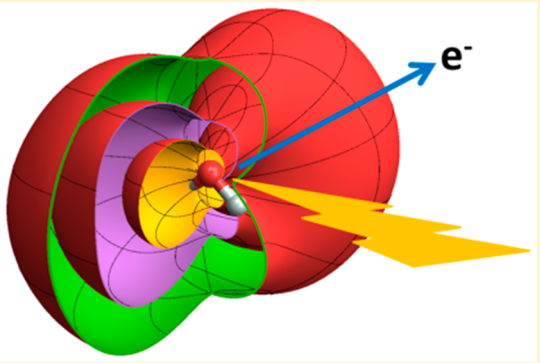

INTRODUCTION

Investigating the dynamics of electrons on their natural time scale requires short, intense laser pulses.[1−3] The angular dependence of strong-field ionization is a process that is governed by electron dynamics on this short time scale. Early work showed that the ionization rate for N_2 and CO differed significantly when the molecule was aligned parallel versus perpendicular to the polarization of the laser field.[4,5] Subsequently, direct measurements of the angular dependence of ionization were performed for N_2, O_2, and CO_2.[6,7] The molecules were aligned with a pump pulse, and the ionization yield was measured as a function of the angle between the polarization of the pump and probe pulses. The angular dependence of ionization of N_2 and O_2 could be described well by single active electron (SAE) approximation, but CO_2 was somewhat problematic.[8] High harmonic generation (HHG) data also yield information about the angular dependence of the ionization rate. Because the amplitudes of the harmonics in HHG spectra depend on the angle of the molecule relative to the laser field, orbital tomography can be used to reconstruct the shape of the highest occupied molecular orbital (HOMO).[9] At higher intensities, HHG spectra also have contributions from lower-lying orbitals.[10−15] These features appear to be the result of direct ionization from lower-lying orbitals rather than excitation of the ion after ionization of the HOMO. Angle-dependent and channel-dependent ionization has also been measured in butadiene and some larger polyatomics.[16−18] Among the hydrides, only H_2O has received a significant amount of attention concerning the angular dependence of ionization.[19−28]

For simple molecules, a qualitative description of the angular dependence of ionization can be obtained from Dyson orbitals, which are computed from the overlap between the neutral and the ionic wave functions, $\Phi_i^D = \int \Psi^{*\text{neutral}} \Psi_i^{\text{cation}} \, d\tau_2 \cdots d\tau_n$. A better description of ionization in the tunneling regime can often be obtained from ADK theory.[29,30] For more quantitative descriptions of HHG and the angular dependence of ionization, the time-dependent Schrödinger equation (TDSE) can be solved with approaches such as SAE-TDSE, quantitative rescattering theory, time-dependent resolution-in-ionic-states, time-dependent analytical R-matrix, and time-dependent generalized active space configuration interaction.[8,31−34] In a previous study, we examined the angle dependence of strong-field ionization for N_2, O_2, CO_2, and CH_2O using a time-dependent configuration interaction (TDCI) approach using atom-centered basis functions.[35] Response properties are described well with the TDCI approach.[28,36−39] Ionization can be simulated if a complex absorbing potential (CAP) is included to absorb the fraction of the electron density that is distorted toward ionization by the laser field.[35,40,41] This approach can treat not only ionization in the tunneling regime but also strong-field ionization by barrier suppression. We compared the TDCI-CAP approach to accurate grid-based calculations and found good agreement for the ionization of H atom as a function of field strength, and the change in the rate of ionization of H_2^+ as a function of bond length.[40] The methodology has been used to study the ionization of ethylene, butadiene, and hexatriene as a function of field strength.[41] By calculating the ionization yield as a function of the direction of polarization of the laser pulse, we obtained three-dimensional surfaces, which correspond to the angle-dependent ionization probabilities. Analysis of the three-dimensional shapes for N_2, O_2, CO_2, and CH_2O showed that ionization occurred not just from the

Received: July 6, 2015
Revised: September 1, 2015
Published: September 9, 2015

DOI: 10.1021/acs.jpca.5b06481
J. Phys. Chem. A 2015, 119, 10212−10220

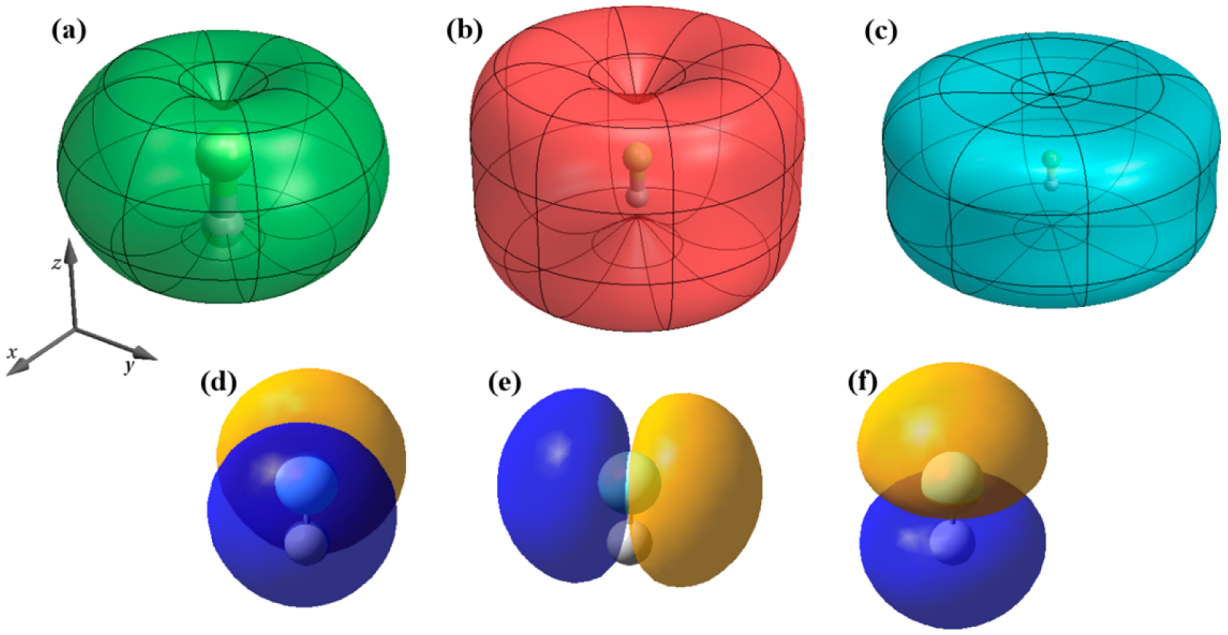

Figure 1. Angular dependence of the ionization yield for HF for a 800 nm seven cycle cosine squared pulse with intensities of (a) 3.51×10^{14} W cm^{-2}, (b) 5.05×10^{14} W cm^{-2}, and (c) 6.87×10^{14} W cm^{-2}, (d, e) the doubly degenerate p_π HOMO and (f) the p_σ HOMO−1 orbital.

HOMO but also from lower-lying orbitals.[35] The Dyson orbitals for the ground state and excited states of the cations provided a satisfactory interpretation of the angle-dependent ionization probabilities.

In the present work, we used the TDCIS-CAP approach to examine the angle-dependent strong-field ionization of a set of second and third period hydrides: BH_3, CH_4, NH_3, H_2O, and HF; AlH_3, SiH_4, PH_3, H_2S, and HCl. These cover a range of shapes and symmetries (linear to T_d) and ionization potentials (10 to 16 eV). The simulations demonstrate that in addition to the HOMO, lower-lying orbitals also contribute to the ionization yield, particularly at higher intensities. Details of the ionization process can be obtained by looking at contributions to the ionization from individual half cycles of the laser pulse and by analyzing the portion of the wave function absorbed by the CAP. Since the results for the third period hydrides are similar to the second period hydrides, they are not discussed separately. The data for AlH_3, SiH_4, PH_3, H_2S, and HCl are collected in the Supporting Information.

METHODS

The electron dynamics were simulated by solving the time-dependent Schrödinger equation

$$i\frac{\partial}{\partial t}\Psi_{el}(t) = [\hat{H}_{el} - \hat{\vec{\mu}}\cdot\vec{E}(t) - i\hat{V}^{absorb}]\Psi_{el}(t) \quad (1)$$

where $\hat{H}_{el}$ is the field-free electronic Hamiltonian. The electron-light interaction is treated in the semiclassical dipole approximation, where $\hat{\vec{\mu}}$ is the dipole operator and $\vec{E}$ is electric field component of the laser pulse. As described in our earlier papers,[35,40,41] the absorbing potential used to model ionization, $-i\hat{V}^{absorb}$ is constructed from a set of overlapping spherical potentials around each atom. A similar form for the complex absorbing potential has recently been used for calculating π^* resonant states.[42] Each spherical potential has a quadratic rise starting at a radius R and a quadratic turnover to constant value of 10 hartree at approximately $R + 7$ Å. At any given point, the total absorbing potential is equal to the minimum of the values from the atomic absorbing potentials. To model ionization, we chose the rise in the CAP to begin at a distance of 3.5 times the van der Waals radius of each element (R_H = 5.051 Å, R_B = 7.145 Å, R_C = 6.739 Å, R_N = 6.405 Å, R_O = 6.125 Å, R_F = 5.887 Å). Because the hydrides are very small molecules, the CAP is nearly spherical and centered on the heavy atom (see Figure 6 for the CAP for H_2O). For the intensities used in Figures 1−8, this choice of radii places the start of the CAP ∼2−4 Å beyond the Coulomb barrier, which is suitable for modeling over the barrier ionization. These radii are a compromise between minimal absorption of the norm in the field-free case and the number of diffuse basis functions needed for interaction with the CAP. The norm in the field-free case is 0.9990 for BH_3, 0.9993 for CH_4, 0.9988 for NH_3, 0.9973 for H_2O, and 0.9985 for HF after an interval of 18.7 fs. Better conservation of the norm for the field-free case and improved representation of the tunneling regime can be achieved by increasing the radii for the CAP but at the cost of adding more diffuse functions.

The time-dependent wave function is expanded in the basis of the Hartree−Fock ground state and all singly excited states of the field-free, time-independent Hamiltonian.

$$\Psi(t) = \sum_{i=0} C_i(t)|\Psi_i\rangle \quad (2)$$

The time-dependent coefficients are propagated using a Trotter factorization of the exponential of the Hamiltonian:

$$\begin{aligned}\Psi(t + \Delta t) &= \exp(-i\hat{\mathbf{H}}\Delta t)\Psi(t)\\ &= \exp(-i\hat{\mathbf{H}}_{el}\Delta t/2)\exp(-\hat{\mathbf{V}}^{absorb}\Delta t/2)\mathbf{W}^T\\ &\quad\times \exp(iE(t + \Delta t/2)\mathbf{d}\Delta t/2)\\ &\quad\times \mathbf{W}\exp(-\hat{\mathbf{V}}^{absorb}\Delta t/2)\exp(-i\hat{\mathbf{H}}_{el}\Delta t/2)\Psi(t)\end{aligned} \quad (3)$$

where $\mathbf{WDW}^T = \mathbf{d}$ are the eigenvalues and eigenvectors of the transition dipole matrix $\mathbf{D}$ in the direction of the polarization of the laser field. $\mathbf{W}$, $\mathbf{d}$, $\exp(-i\hat{\mathbf{H}}_{el}\Delta t)$, and $\exp(\hat{\mathbf{V}}^{absorb}\Delta t/2)$ need to be calculated only once because they are time-independent. The propagation involves a pair of matrix-vector product and the exponential of the diagonal matrix, $\mathbf{d}$. A time step of Δt = 1.2 as

DOI: 10.1021/acs.jpca.5b06481
J. Phys. Chem. A 2015, 119, 10212−10220

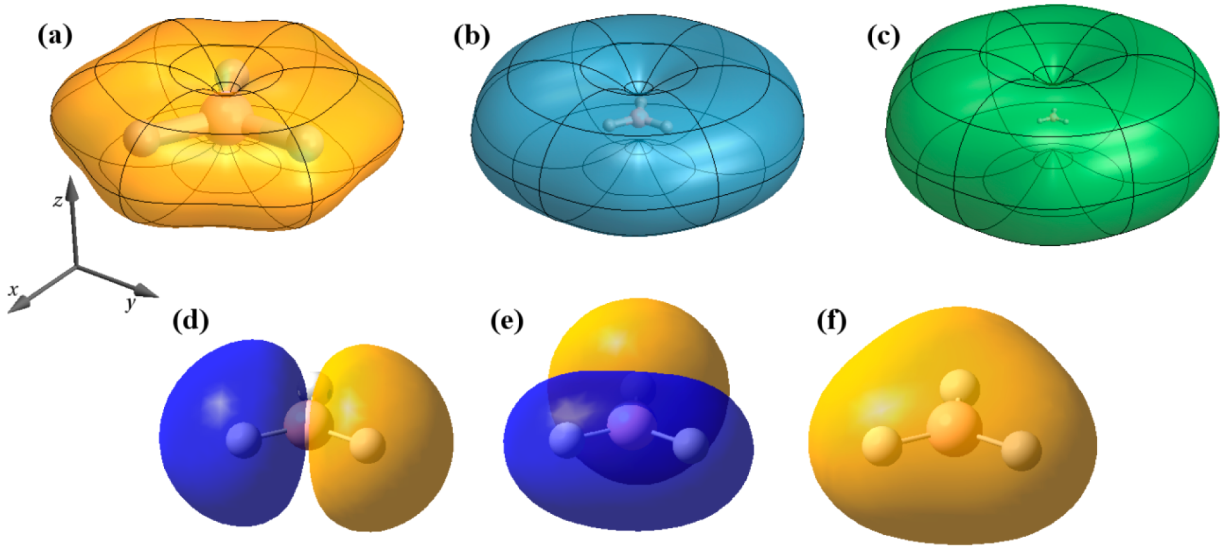

Figure 2. Angular dependence of the ionization yield for BH_3 for a 800 nm seven cycle cosine squared pulse with intensities of (a) 1.26×10^{14} W cm^{-2}, (b) 2.25×10^{14} W cm^{-2}, (c) 3.51×10^{14} W cm^{-2}, (d, e) the doubly degenerate HOMO, and (f) HOMO−1.

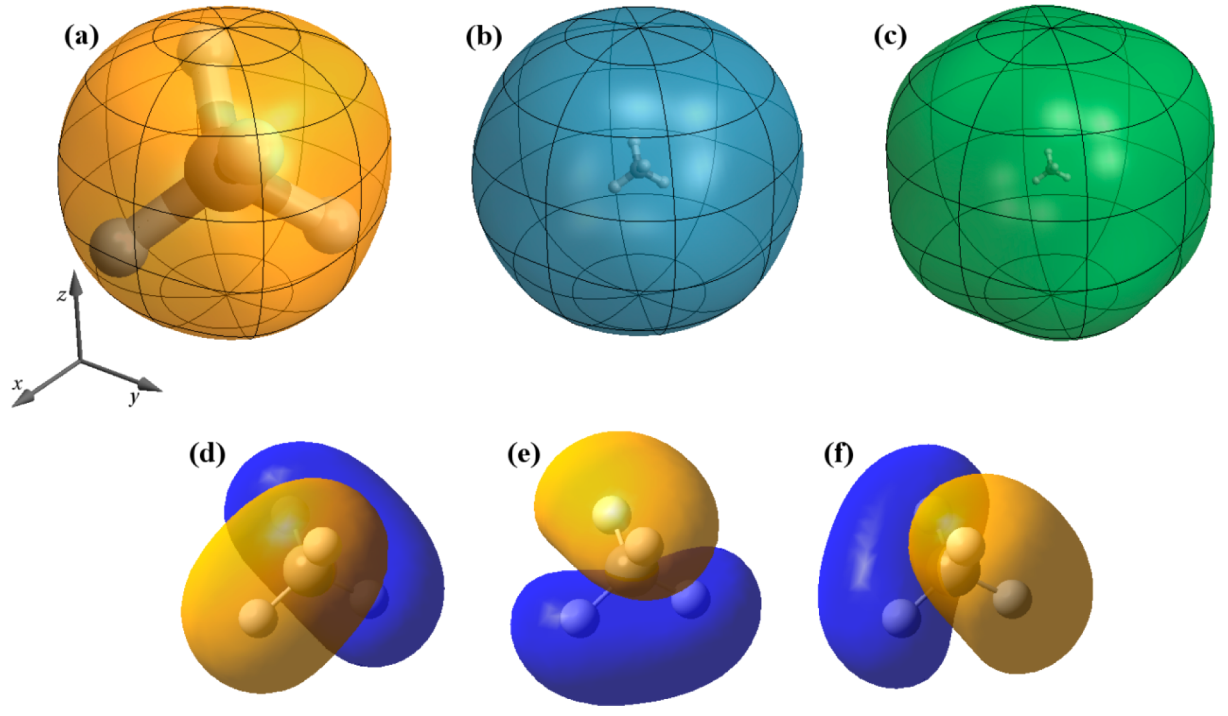

Figure 3. Angular dependence of the ionization yield for CH_4 for a 800 nm seven cycle cosine squared pulse with intensities of (a) 1.26×10^{14} W cm^{-2}, (b) 2.25×10^{14} W cm^{-2}, and (c) 3.51×10^{14} W cm^{-2}, (d–f) the triply degenerate HOMO.

(0.05 au) was used for the propagation. Earlier tests showed that reducing the time step by a factor of 2 changed the norm at the end of the pulse by less than 0.1%.[40]

The electronic structure calculations were performed with a locally modified version of the Gaussian program package.[43] The standard Dunning aug-cc-pVTZ basis[44,45] was augmented with an absorbing basis containing extra diffuse functions to ensure sufficient interaction with the CAP. This absorbing basis consisted of nine sets of diffuse Gaussian functions on each atom (including hydrogens): three *s* functions (with exponents: 0.0256, 0.0128, and 0.0064), two sets of *p* functions (0.0256, 0.0128), three sets of pure *d* functions (0.0512, 0.0256, and 0.0128), and one set of pure *f* functions (0.0256). For the most diffuse functions, the matrix elements of $\hat{\mathbf{V}}^{\text{absorb}}$ are of the order of 0.1, and the largest eigenvalues of the $\hat{\mathbf{V}}^{\text{absorb}}$ matrix are of the order of 0.5. Details of the development and testing of the absorbing basis can be found in ref 40. In particular, this choice of exponents and CAP radii yields good agreement with accurate grid-based calculations for the ionization of H atom as a function of field strength and the change in the rate of ionization of H_2^+ as a function of bond length.[40]

The simulations used a seven cycle, linearly polarized cosine squared pulse

$$E(t) = E_{\text{max}}\cos^2(\pi t/2\sigma)\cos(\omega t + \phi) \text{ for } -\sigma \le t \le \sigma$$
$$E(t) = 0 \text{ otherwise} \quad (4)$$

DOI: 10.1021/acs.jpca.5b06481
J. Phys. Chem. A 2015, 119, 10212−10220

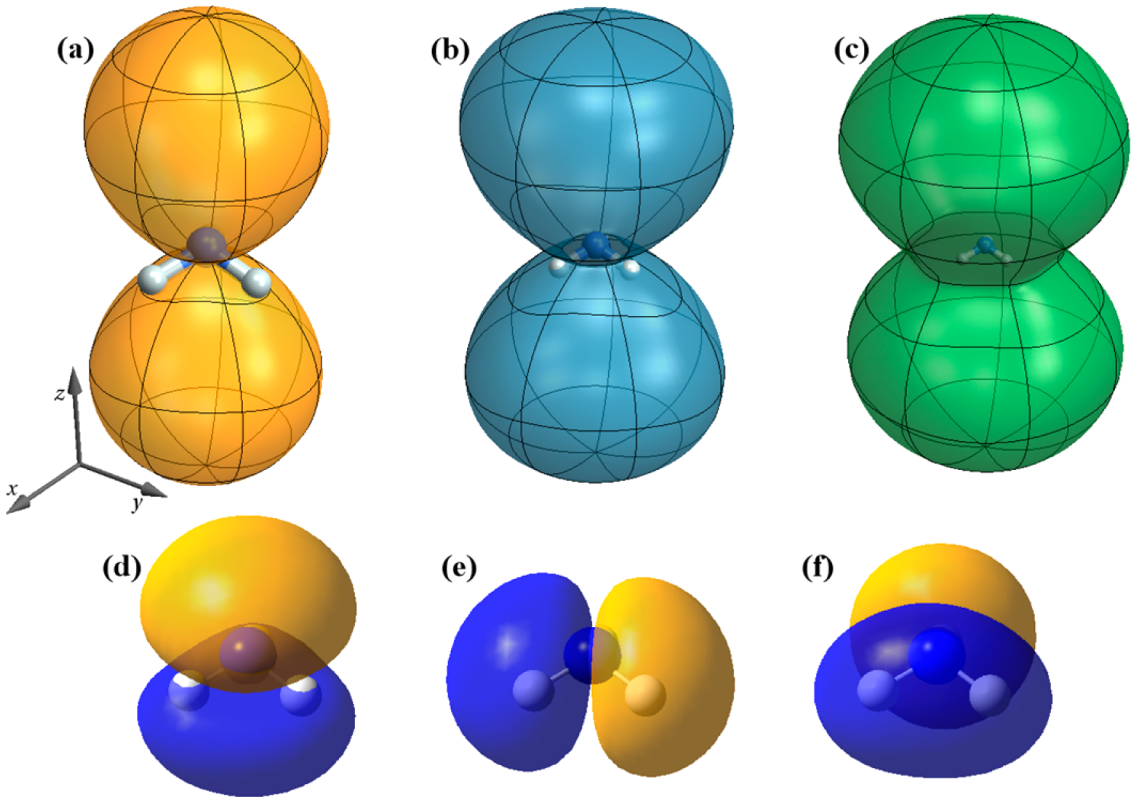

Figure 4. Angular dependence of the ionization yield for NH_3 for a 800 nm seven cycle cosine squared pulse with intensities of (a) 1.26×10^{14} W cm^{-2}, (b) 2.25×10^{14} W cm^{-2}, (c) 3.51×10^{14} W cm^{-2}, (d) the HOMO, (e, f) the double degenerate HOMO−1.

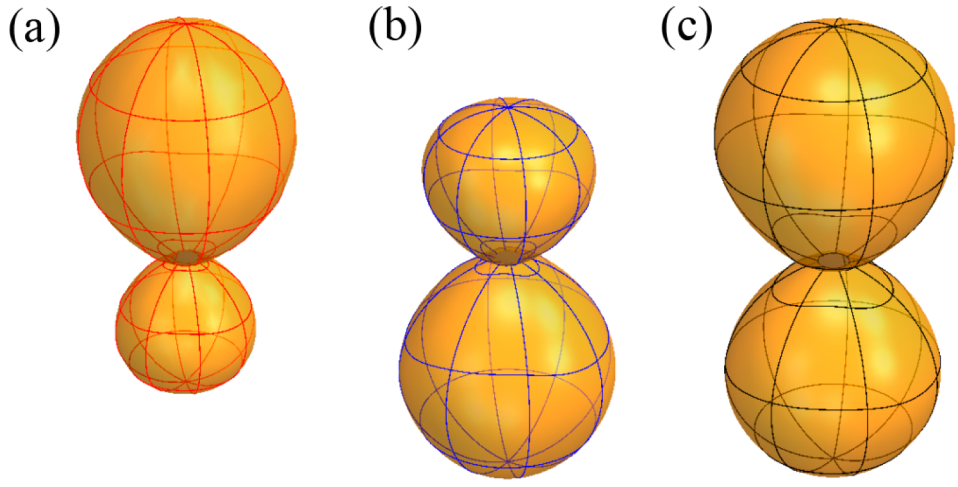

Figure 5. Angular dependence of the ionization yield for NH_3 for (a) the first half of the optical cycle in the middle of the seven cycle pulse, (b) the second half of optical cycle, and (c) the full optical cycle with an intensity of 1.26×10^{14} W cm^{-2} (see Figure 7a for a plot of the laser pulse).

with a wavelength of 800 nm (9.35 fs fwhm) and $\phi = \pi$ (the shape of the pulse can be seen in Figure 7a). The system was propagated for 24.2 fs (1000 au) with intensities from 0.56×10^{14} to 7.90×10^{14} W cm^{-2} (electric field strengths from 0.04 to 0.15 au). Since the HOMO, HOMO−1, and HOMO−2 orbital energies for BH_3, CH_4, NH_3, H_2O, and HF are in the range from −0.43 to −0.77 hartree, ionization with these intensities occurs primarily by barrier suppression rather than by tunneling. The loss of norm was calculated after the pulse (18.7 fs) when the field has returned to zero and is taken as the ionization yield for the pulse. By varying the polarization direction of the pulse with a given E_{max}, we obtain a three-dimensional surface, which we interpret as an angle-dependent ionization probability. For each molecule, three values of E_{max} were chosen to cover a range of ionization yields. Up to 114 points were calculated for each E_{max}, and three-dimensional plots were generated using the ionization yield as the radial distance and the direction of the polarization as the angles. For the lower E_{max} in each set, the radial distances were scaled so that the shape of the surface would not be obscured by the molecular structure. To obtain smooth surfaces, the ionization yields as a function of the angles were fitted to polynomials in $\cos(\theta)^n \cos(m\varphi)$ and $\cos(\theta)^n \sin(m\varphi)$, $n = 0–9$, $m = 0–4$.

DOI: 10.1021/acs.jpca.5b06481
J. Phys. Chem. A 2015, 119, 10212−10220

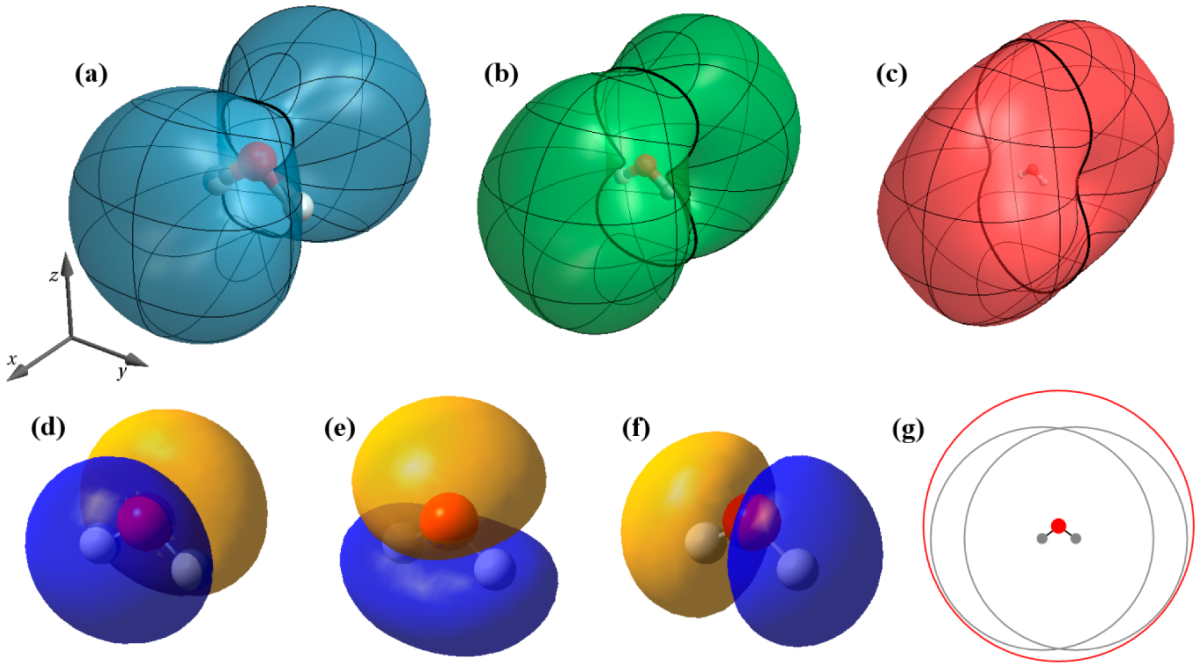

Figure 6. Angular dependence of the ionization yield for H_2O for a 800 nm seven cycle cosine squared pulse with intensities of (a) 2.25×10^{14} W cm^{-2} and (b) 3.51×10^{14} W cm^{-2}, (c) 5.05×10^{14} W cm^{-2}, and (d) HOMO, (e) HOMO−1, (f) HOMO−2, and (g) CAP for H_2O constructed from spheres with radii R_O and R_H.

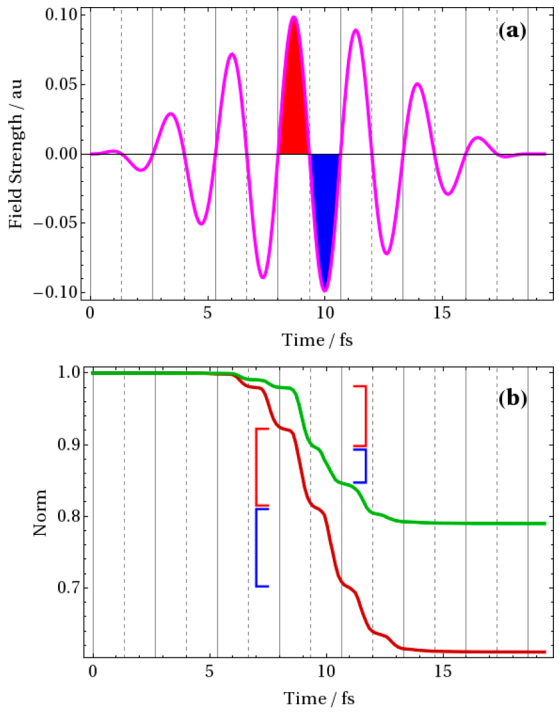

Figure 7. (a) Shape of the pulse (highlighted in red and blue are the half cycles in the middle of the pulse), and (b) loss of norm for H_2O with polarization of the pulse in the x (green) and z (red) directions (perpendicular to the plane and along the C_2 axis, respectively) for a 800 nm seven cycle cosine squared pulse with an intensity of 2.25×10^{14} W cm^{-2}. In (b) the drop in norm during the first half cycle is highlighted by the red brackets, and during the second half cycle by the blue brackets.

RESULTS AND DISCUSSION

The angular dependence of the ionization yield for hydrogen fluoride is shown in Figure 1. The HOMO consists of a doubly degenerate pair of p_π orbitals; the Dyson orbital is nearly identical to the HOMO. HF has the highest ionization potential of the hydrides and therefore needs the highest intensity pulse to achieve a suitable rate of ionization. As expected from the doubly degenerate HOMO, the angular dependence of the ionization yield is cylindrically symmetrical about the molecular axis. At lower intensities, there is a minimum along the molecular axis, but at higher intensities, one can see increasing contributions from the p_σ HOMO−1. Comparable results are found for HCl (Figure S1 in the Supporting Information).

Figure 2 shows the results for BH_3. Ionization is mainly in the plane of the molecule, with very little ionization along axis perpendicular to the molecular plane. The HOMO is the doubly degenerate combination of the B−H bond orbitals; the Dyson orbital looks the same as HOMO. The superposition of the electron density from the degenerate HOMOs is highest in the plane of the molecule and has a shape similar to the angular dependence of the ionization. With increasing intensity the shape evolves from hexagonal to nearly circular. For methane (Figure 3), there is relatively little angular variation in the ionization yield at low intensities. At higher intensities, the ionization yield has features with O_h symmetry. The triply degenerate HOMO is a combination of the C−H bond orbitals. The superposition of the densities of three degenerate orbitals gives a probability distribution with T_d symmetry (however, see the discussion below). The results for AlH_3 and SiH_4 are similar to those for BH_3 and CH_4, respectively (Figure S1).

The strong-field ionization of ammonia is dominated by removal of an electron from the HOMO, an sp^3 lone pair orbital. Figure 4 shows that the angular dependence of ionization yield for NH_3 looks more like a p-orbital (the same is found for PH_3, Figure S1). The more symmetrical shape is a direct consequence of the linearly polarized laser field oscillating between positive and negative values. This can be illustrated by calculating the ionization yield for a series of half cycles, as shown in Figure 5. For a continuous (CW) laser field, the same electric field can be

DOI: 10.1021/acs.jpca.5b06481
J. Phys. Chem. A 2015, 119, 10212−10220

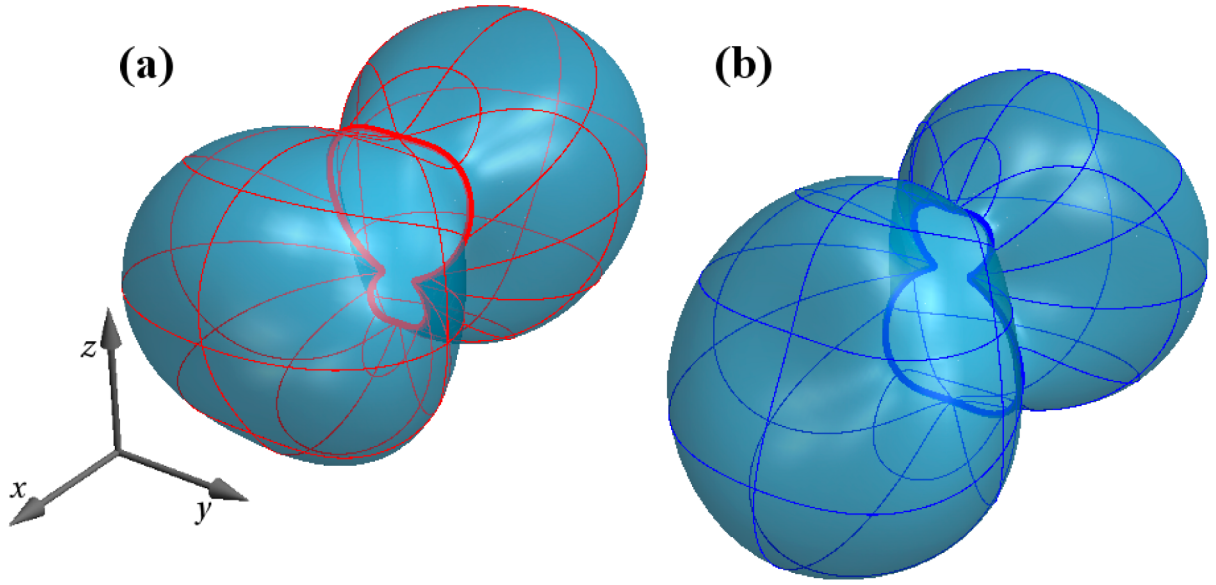

Figure 8. Angular dependence of the ionization yield for H_2O (a) the first half of the optical cycle in the middle of the seven cycle pulse (red mesh lines), and (b) the second half of optical cycle (blue mesh lines) for a 800 nm seven cycle cosine squared pulse with an intensity of 2.25×10^{14} W cm^{-2}.

obtained by advancing half a cycle and inverting the polarization direction (i.e., rotating the polarization by 180°). Hence, after advancing half a cycle the angular dependence of the ionization yield on the laser polarization direction is also inverted (slightly diminished because of the finite amount of ionization during each half cycle). For a cosine squared pulse with $\phi = \pi$, this also holds for the two half cycles in the middle of the pulse (see Figure 7a). The result from the first half of the optical cycle taken from the middle of the seven cycle pulse is shown in Figure 5a. The angular dependence of the ionization yield looks similar to an sp^3 lone pair. In the next half cycle, Figure 5b, the field has changed sign, but the same field can be obtained by inverting the polarization (rotating the polarization by 180°). Hence the angular dependence of the ionization yield is inverted and looks like the sp^3 lone pair inverted through the origin. When the full cycle is considered, Figure 5a,b, the sum of the two half cycles looks like a p_π orbital. Thus, the angular dependence of the ionization yield for polyatomics should not be compared to the HOMO or the corresponding Dyson orbital but should be compared to the density from the HOMO or Dyson orbital plus this density inverted through the origin. The approximate inversion symmetry of the angular dependence of the ionization yield has been discussed previously.[23] For BH_3, applying inversion symmetry to the electron density of the doubly degenerate HOMO (D_{3h}) results in D_{6h} symmetry, which matches the shape of the ionization yield, Figure 2a. Likewise for CH_4, summing the densities from the triply degenerate HOMOs yields T_d symmetry; applying inversion symmetry produces a distribution that has O_h symmetry and resembles the ionization yield at high intensities, Figure 3c.

For water, the angular dependence of ionization yield is dominated by the p_π lone pair HOMO, as shown in Figure 6 (the similar shapes are seen for H_2S, Figure S1). Closer inspection of the ionization yield in the plane of the molecule shows that there is also some contribution from the in-plane sp^2 lone pair, HOMO−1. This contribution increases as the intensity is increased. The shape of the laser pulse and evolution of the wave function norm are illustrated in Figure 7 for polarization in the x and z directions. For polarization perpendicular to the plane (x direction), the norm decreases by the same amount during the first half cycle and the second half cycle in the middle of the pulse (left-hand red and blue brackets, respectively, in Figure 7b). However, for polarization along the C_2 axis ($+z$ direction), the loss of norm is larger in the first half cycle than in the second half cycle (right-hand red and blue brackets, respectively, in Figure 7b), reflecting the fact that the sp^2 lone pair is larger in one direction along the axis than in the opposite direction. More detail can be seen by using only the first half cycle of a pulse to obtain the angular dependence of the ionization yield, Figure 8. For the polarization in the plane of the molecule (highlighted in Figure 8), the loss of norm of the wave function clearly shows the larger and smaller lobes of the sp^2 lone pair. If the second half of the optical cycle is used, the curve is inverted. The sum of the two curves reproduces the shape of the ionization yield seen in the plane of the molecule, as shown in Figure 6a.

Although strong-field ionization is dominated by loss of an electron from the HOMO, there is abundant experimental and computational evidence for direct ionization from lower-lying orbitals.[10−15] For the TDCI-CAP approach, the nature of the ions produced can be probed by analyzing the portion of the wave function that is absorbed by the CAP. At any given point in time during the simulation, the change in the wave function when multiplied by CAP is characteristic of the ion produced at that instant, and the change in norm is related to the instantaneous ionization rate.

$$\tilde{\Psi}(t)_{\text{ion}} \approx \Psi(t)_{\text{neutral}} - \exp(-\hat{V}^{\text{absorb}}\Delta t)\Psi(t)_{\text{neutral}}$$
$$\Psi(t)_{\text{ion}} = \tilde{\Psi}(t)_{ion}/|\tilde{\Psi}(t)_{\text{ion}}|$$
$$\text{rate}(t) \propto |\tilde{\Psi}(t)_{\text{ion}}|/\Delta t \quad (5)$$

This difference in the wave function, $\Psi(t)_{\text{ion}}$, can be analyzed in terms of its one electron density matrix and instantaneous molecular orbital populations, $p_i(t)$. Integration over the pulse gives an average over the populations of the ions produced.

$$\Psi(t)_{\text{ion}} \Rightarrow p_i(t)$$
$$p_i = \int \text{rate}(t)p_i(t)\text{d}t / \int \text{rate}(t)\text{d}t \quad (6)$$

DOI: 10.1021/acs.jpca.5b06481
J. Phys. Chem. A 2015, 119, 10212−10220

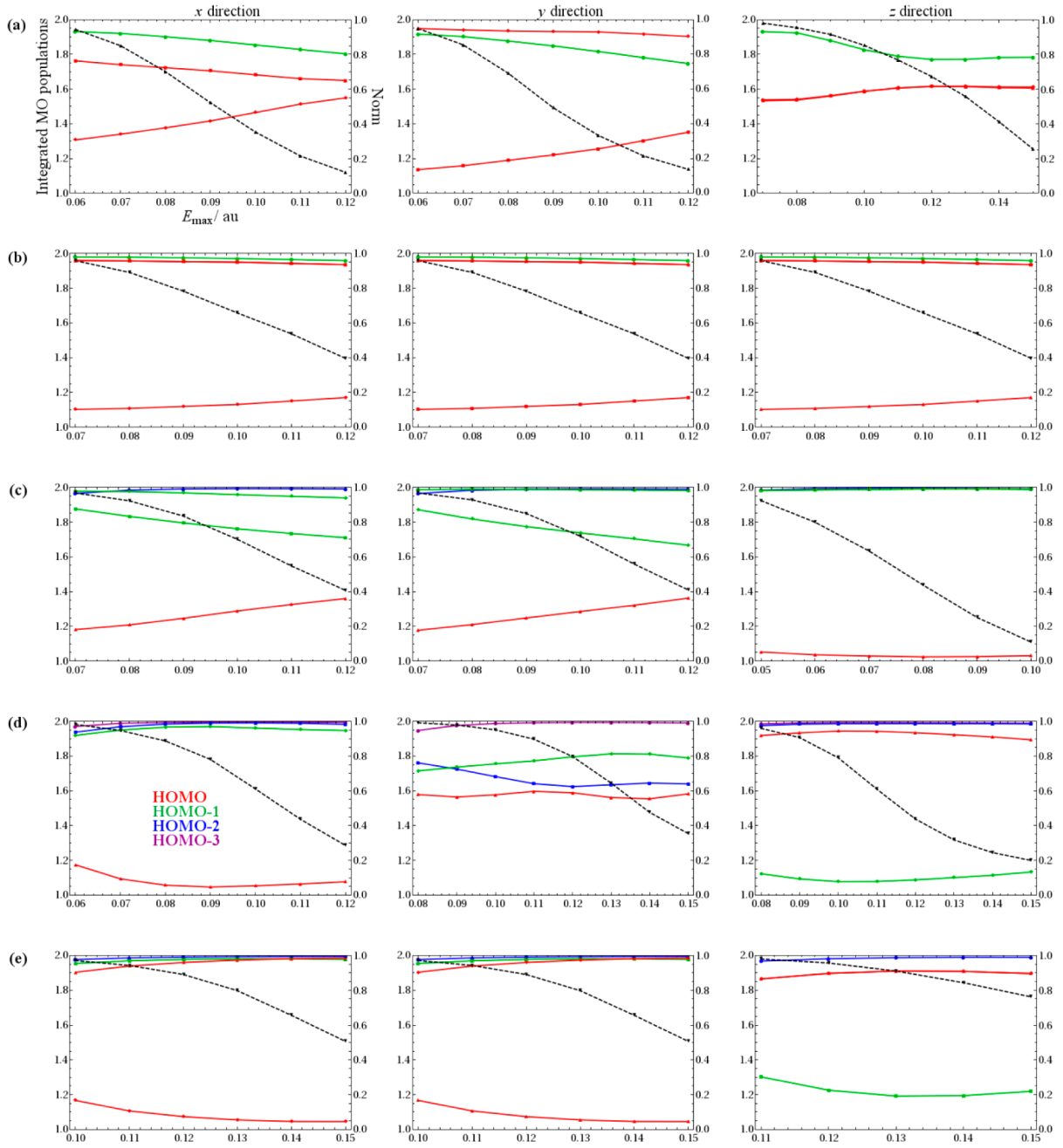

Figure 9. Orbital populations resulting from ionization by a 800 nm seven cycle cosine squared pulse with polarization along the *x*, *y*, and *z* directions. The populations (left-hand axis) of the HOMO (red), HOMO−1 (green), HOMO−2 (blue), and HOMO−3 (purple) are shown for (a) BH_3, (b) CH_4, (c) NH_3, (d) H_2O, and (e) HF as a function of field strength. Also shown are the corresponding decreases in the norms of the neutral wave function as a function of the field strengths (dashed black lines, right-hand axis).

For low field strengths, the loss of norm of the neutral wave function is very small, and the results are skewed by the field-free absorption of the wave function by the CAP. Meaningful populations are obtained if the norm of the neutral wave function after the pulse is ∼0.98 or less.

The orbital populations of the ions and the norm of the neutral wave function for the second period hydrides are plotted as a function of field strength in Figure 9 for selected orientations of the laser polarization. The corresponding results for the third period hydrides can be found in Figure S2. The results for HF are perhaps the easiest to understand. Because of the high ionization potential of HF, high field strengths are necessary to see a significant decrease in norm of the neutral wave function. For laser polarizations in the *x* and *y* directions (Figure 9e, perpendicular to the molecular axis), the population of the p_π HOMO is depleted (orbital energy −0.652 hartree), as expected. When the polarization is along the molecular axis (*z* direction), the p_σ HOMO−1 (orbital energy −0.776 hartree) is the major contributor. This agrees with the deductions based on the shapes of the angular dependence of the ionization shown in Figure 1.

Ionization of BH_3 is dominated by removal of electrons from the HOMO (Figure 9a). To achieve a suitable amount of ionization (i.e., drop in norm of the neutral wave function), a larger field strength is need when the polarization is perpendicular to the molecular plane (*z* direction) than when it is in the plane of the molecule (*x* and *y* directions). The two degenerate orbitals of

DOI: 10.1021/acs.jpca.5b06481
J. Phys. Chem. A 2015, 119, 10212−10220

the HOMO (orbital energy −0.499 hartree) contribute equally for polarization in the z direction, but this degeneracy is lifted when the polarization is in the x and y directions. At higher field strengths, the contribution from HOMO−1 increases (orbital energy −0.705 hartree). The analysis of the populations is in agreement with the qualitative analysis of the angular dependence of the ionization shown in Figure 2.

For ionization of CH_4, polarization in the x, y, and z directions removes an electron from different orbitals in the triply degenerate t_2 HOMO (orbital energy −0.546 hartree) shown in Figure 9b. For higher field strengths there is a slight increase in the contributions from the other t_2 HOMO orbitals and the a_1 HOMO−1 (this is more pronounced for SiH_4). For NH_3 and PH_3 in Figures 9c and S2, the lone pair HOMOs (orbital energies −0.426 and −0.382 hartree, respectively) are the only contributors for polarization along the molecular axis (z direction) at all field strengths considered. However, for polarization perpendicular to the axis (x and y directions), contributions from HOMO−1 of NH_3 and PH_3 (orbital energy −0.637 and −0.528 hartree, respectively) are seen to increase with increasing field strength.

Because of their lower symmetry, the orbital populations of H_2O and H_2S show more diverse behavior when the polarization of the ionizing pulse is in the x, y, and z directions (Figures 9d and S2). As expected, when the field is in the x direction ionization is dominated by removal of an electron from the p_π HOMO (orbital energies −0.511 and −0.385 hartree for H_2O and H_2S, respectively). Likewise, the sp^2 lone pair HOMO−1 (orbital energies −0.585 and −0.499 hartree, respectively) dominates when the field is in the z direction, but a higher field strength is needed to achieve a comparable amount of ionization (i.e., drop in norm of the neutral wave function). Aligning the laser polarization with the y direction gives a mixture of ionization from the three highest occupied orbitals.

In terms of the angular dependence of ionization of polyatomic hydrides, H_2O has received the most attention.[19−28] Weak field asymptotic theory has been used to study the angle dependence of tunneling ionization by a static field.[19] Molecular ADK theory[30] was employed to calculate the orientation dependence of tunneling ionization for a series of polyatomic molecules, including H_2O.[20] Molecular strong-field approximation[46,47] has been used to examine the ionization of H_2O fixed in space.[21] While the HOMO dominates at most angles, HOMO−1 is the major contributor when the laser polarization is along the symmetry axis. Son and Chu[22] have studied the orientation-dependent ionization of water using a grid-based time-dependent density functional theory with proper long-range behavior. While the HOMO dominates for orientations out of the plane of the molecule, HOMO−1 determines the shape for laser polarizations in the plane of the molecule. Small contributions are also seen from HOMO−2. The present calculations are in good agreement with these findings. Petretti et al.[23] have examined the ionization of water by solving the time-dependent Schrödinger equation in the single active electron approximation. They also found that the HOMO dominated the overall shape of the ionization, but HOMO−1 determined the shape of the ionization yield within the molecular plane. For short pulses, they found that the angular dependence of the ionization was affected by the carrier envelope phase. In the present calculations, we also find a pronounced phase dependence by using a half cycle pulse to scan the angular dependence of ionization (Figures 5, 7, and 8). Ionization of water by half cycle pulses was also studied by Borbely et al.[24]

Experimental studies of high harmonic generation (HHG) for water found harmonics beyond the expected cutoff.[25] This was attributed to suppression of ionization because of the nodal plane in the HOMO. The comparison of HHG spectra of H_2O and D_2O provides evidence of ionization from HOMO−1.[26] While ionization from the HOMO results in almost no change in the geometry, ionization from HOMO−1 produces a large change in the angle leading to the isotope effect seen in the experimental HHG spectra.[26,27] Calculations with time-dependent configuration interaction with single and double excitations showed that HHG spectrum for H_2O also contained even harmonics when the field was applied along the molecular symmetry axis.[28]

CONCLUSIONS

The angular dependence of strong-field ionization for a set of second period hydrides (BH_3, CH_4, NH_3, H_2O, and HF) and third period hydrides (AlH_3, SiH_4, PH_3, H_2S, and HCl) has been simulated using time-dependent configuration interaction with a complex absorbing potential (TDCIS-CAP). The molecules were subject to seven cycle 800 nm cosine squared pulse laser pulse, and the drop in norm of the wave function of the neutral was used as a measure of the ionization yield. At low intensities, the angular dependence is dominated by the shape of the electron density of highest occupied orbital plus this density inverted through the origin. With increasing intensity, changes in the shape of the ionization yield indicate contributions from lower-lying orbitals. This is most easily seen when the laser polarization is in the nodal plane of the HOMO. Population analysis of the component of the wave function absorbed by the complex absorbing potential reveals the dependence of ionization from the HOMO and lower-lying orbitals on the laser intensity and polarization direction.

ASSOCIATED CONTENT

Supporting Information

The Supporting Information is available free of charge on the ACS Publications website at DOI: 10.1021/acs.jpca.5b06481.

Plots of the angular dependence of the ionization yield and orbital populations resulting from ionization for AlH_3, SiH_4, PH_3, H_2S, and HCl. Absorbing basis set information and Cartesian coordinates of the molecules. (PDF)

AUTHOR INFORMATION

Corresponding Author

*E-mail: hbs@chem.wayne.edu.

Notes

The authors declare no competing financial interest.

ACKNOWLEDGMENTS

This work was supported by grants from the National Science Foundation (CHE1212281, CHE1464450). We thank Wayne State University's computing grid for computer time.

REFERENCES

(1) Kling, M. F.; Vrakking, M. J. J. Attosecond electron dynamics. *Annu. Rev. Phys. Chem.* **2008**, *59*, 463−492.

(2) Krausz, F.; Ivanov, M. Attosecond physics. *Rev. Mod. Phys.* **2009**, *81*, 163−234.

(3) Gallmann, L.; Cirelli, C.; Keller, U. Attosecond science: Recent highlights and future trends. *Annu. Rev. Phys. Chem.* **2012**, *63*, 447−469.

(4) Litvinyuk, I. V.; Lee, K. F.; Dooley, P. W.; Rayner, D. M.; Villeneuve, D. M.; Corkum, P. B. Alignment-dependent strong field ionization of molecules. *Phys. Rev. Lett.* **2003**, *90*, 233003.

(5) Pinkham, D.; Jones, R. R. Intense laser ionization of transiently aligned CO. *Phys. Rev. A: At., Mol., Opt. Phys.* **2005**, *72*, 023418.

(6) Pavicic, D.; Lee, K. F.; Rayner, D. M.; Corkum, P. B.; Villeneuve, D. M. Direct measurement of the angular dependence of ionization for N_2, O_2, and CO_2 in intense laser fields. *Phys. Rev. Lett.* **2007**, *98*, 243001.
(7) Thomann, I.; Lock, R.; Sharma, V.; Gagnon, E.; Pratt, S. T.; Kapteyn, H. C.; Murnane, M. M.; Li, W. Direct measurement of the angular dependence of the single-photon ionization of aligned N_2 and CO_2. *J. Phys. Chem. A* **2008**, *112*, 9382−9386.
(8) Petretti, S.; Vanne, Y. V.; Saenz, A.; Castro, A.; Decleva, P. Alignment-Dependent Ionization of N_2, O_2, and CO_2 in Intense Laser Fields. *Phys. Rev. Lett.* **2010**, *104*, 223001.
(9) Itatani, J.; Levesque, J.; Zeidler, D.; Niikura, H.; Pepin, H.; Kieffer, J. C.; Corkum, P. B.; Villeneuve, D. M. Tomographic imaging of molecular orbitals. *Nature* **2004**, *432*, 867−871.
(10) McFarland, B. K.; Farrell, J. P.; Bucksbaum, P. H.; Guhr, M. High harmonic generation from multiple orbitals in N_2. *Science* **2008**, *322*, 1232−1235.
(11) Smirnova, O.; Mairesse, Y.; Patchkovskii, S.; Dudovich, N.; Villeneuve, D.; Corkum, P.; Ivanov, M. Y. High harmonic interferometry of multi-electron dynamics in molecules. *Nature* **2009**, *460*, 972−977.
(12) Le, A. T.; Lucchese, R. R.; Lin, C. D. Uncovering multiple orbitals influence in high harmonic generation from aligned N_2. *J. Phys. B: At., Mol. Opt. Phys.* **2009**, *42*, 211001.
(13) Jin, C.; Bertrand, J. B.; Lucchese, R. R.; Worner, H. J.; Corkum, P. B.; Villeneuve, D. M.; Le, A. T.; Lin, C. D. Intensity dependence of multiple orbital contributions and shape resonance in high-order harmonic generation of aligned N_2 molecules. *Phys. Rev. A: At., Mol., Opt. Phys.* **2012**, *85*, 013405.
(14) Zhang, J. T.; Wu, Y.; Zeng, Z. N.; Xu, Z. Z. Intensity-dependent multiorbital effect in high-order harmonics generated from aligned O_2 molecules. *Phys. Rev. A: At., Mol., Opt. Phys.* **2013**, *88*, 033826.
(15) Li, J. W.; Liu, P.; Yang, H.; Song, L. W.; Zhao, S. T.; Lu, H.; Li, R. X.; Xu, Z. Z. High harmonic spectra contributed by HOMO-1 orbital of aligned CO_2 molecules. *Opt. Express* **2013**, *21*, 7599−7607.
(16) Boguslavskiy, A. E.; Mikosch, J.; Gijsbertsen, A.; Spanner, M.; Patchkovskii, S.; Gador, N.; Vrakking, M. J. J.; Stolow, A. The Multielectron ionization dynamics underlying attosecond strong-field spectroscopies. *Science* **2012**, *335*, 1336−1340.
(17) Mikosch, J.; Boguslavskiy, A. E.; Wilkinson, I.; Spanner, M.; Patchkovskii, S.; Stolow, A. Channel- and angle-resolved above threshold ionization in the molecular frame. *Phys. Rev. Lett.* **2013**, *110*, 023004.
(18) Njoya, O.; Matsika, S.; Weinacht, T. Angle-resolved strong-field ionization of polyatomic molecules: More than the orbitals matters. *ChemPhysChem* **2013**, *14*, 1451−1455.
(19) Madsen, L. B.; Jensen, F.; Tolstikhin, O. I.; Morishita, T. Application of the weak-field asymptotic theory to tunneling ionization of H_2O. *Phys. Rev. A: At., Mol., Opt. Phys.* **2014**, *89*, 033412.
(20) Zhao, S. F.; Xu, J. L.; Jin, C.; Le, A. T.; Lin, C. D. Effect of orbital symmetry on the orientation dependence of strong field tunnelling ionization of nonlinear polyatomic molecules. *J. Phys. B: At., Mol. Opt. Phys.* **2011**, *44*, 035601.
(21) Picca, R. D.; Fiol, J.; Fainstein, P. D.; Hansen, J. P.; Dubois, A. Laser pulse ionization of fixed-in-space H_2O. *J. Phys. B: At., Mol. Opt. Phys.* **2012**, *45*, 194009.
(22) Son, S. K.; Chu, S. I. Theoretical study of orientation-dependent multiphoton ionization of polyatomic molecules in intense ultrashort laser fields: A new time-dependent Voronoi-cell finite difference method. *Chem. Phys.* **2009**, *366*, 91−102.
(23) Petretti, S.; Saenz, A.; Castro, A.; Decleva, P. Water molecules in ultrashort intense laser fields. *Chem. Phys.* **2013**, *414*, 45−52.
(24) Borbely, S.; Tokesi, K.; Nagy, L. Ionization of the water by intense ultrashort half-cycle electric pulses. *Eur. Phys. J. D* **2010**, *59*, 337−348.
(25) Wong, M. C. H.; Brichta, J. P.; Bhardwaj, V. R. High-harmonic generation in H_2O. *Opt. Lett.* **2010**, *35*, 1947−1949.
(26) Farrell, J. P.; Petretti, S.; Förster, J.; McFarland, B. K.; Spector, L. S.; Vanne, Y. V.; Decleva, P.; Bucksbaum, P. H.; Saenz, A.; Gühr, M. Strong field ionization to multiple electronic states in water. *Phys. Rev. Lett.* **2011**, *107*, 083001.
(27) Rao, B. J.; Varandas, A. J. C. Subfemtosecond Quantum Nuclear Dynamics in Water Isotopomers. *J. Phys. Chem. A* **2015**, *119*, 4856−4863.
(28) Krause, P.; Klamroth, T.; Saalfrank, P. Molecular response properties from explicitly time-dependent configuration interaction methods. *J. Chem. Phys.* **2007**, *127*, 034107.
(29) Ammosov, M. V.; Delone, N. B.; Krainov, V. P. Tunnel ionization of complex atoms and of atomic ions in an alternating electromagnetic field. *Soviet Physics - JETP* **1986**, *64*, 1191−1194.
(30) Tong, X. M.; Zhao, Z. X.; Lin, C. D. Theory of molecular tunneling ionization. *Phys. Rev. A: At., Mol., Opt. Phys.* **2002**, *66*, 033402.
(31) Le, A. T.; Lucchese, R. R.; Tonzani, S.; Morishita, T.; Lin, C. D. Quantitative rescattering theory for high-order harmonic generation from molecules. *Phys. Rev. A: At., Mol., Opt. Phys.* **2009**, *80*, 013401.
(32) Spanner, M.; Patchkovskii, S. One-electron ionization of multielectron systems in strong nonresonant laser fields. *Phys. Rev. A: At., Mol., Opt. Phys.* **2009**, *80*, 063411.
(33) Torlina, L.; Ivanov, M.; Walters, Z. B.; Smirnova, O. Time-dependent analytical R-matrix approach for strong-field dynamics. II. Many-electron systems. *Phys. Rev. A: At., Mol., Opt. Phys.* **2012**, *86*, 043409.
(34) Bauch, S.; Sorensen, L. K.; Madsen, L. B. Time-dependent generalized-active-space configuration-interaction approach to photo-ionization dynamics of atoms and molecules. *Phys. Rev. A: At., Mol., Opt. Phys.* **2014**, *90*, 062508.
(35) Krause, P.; Schlegel, H. B. Angle-dependent ionization of small molecules by time-dependent configuration interaction and an absorbing potential. *J. Phys. Chem. Lett.* **2015**, *6*, 2140−2146.
(36) Schlegel, H. B.; Smith, S. M.; Li, X. S. Electronic optical response of molecules in intense fields: Comparison of TD-HF, TD-CIS, and TD-CIS(D) approaches. *J. Chem. Phys.* **2007**, *126*, 244110.
(37) Breidbach, J.; Cederbaum, L. S. Migration of holes: Numerical algorithms and implementation. *J. Chem. Phys.* **2007**, *126*, 034101.
(38) Mignolet, B.; Levine, R. D.; Remacle, F. Localized electron dynamics in attosecond-pulse-excited molecular systems: Probing the time-dependent electron density by sudden photoionization. *Phys. Rev. A: At., Mol., Opt. Phys.* **2012**, *86*, 053429.
(39) Luppi, E.; Head-Gordon, M. The role of Rydberg and continuum levels in computing high harmonic generation spectra of the hydrogen atom using time-dependent configuration interaction. *J. Chem. Phys.* **2013**, *139*, 164121.
(40) Krause, P.; Sonk, J. A.; Schlegel, H. B. Strong field ionization rates simulated with time-dependent configuration interaction and an absorbing potential. *J. Chem. Phys.* **2014**, *140*, 174113.
(41) Krause, P.; Schlegel, H. B. Strong-field ionization rates of linear polyenes simulated with time-dependent configuration interaction with an absorbing potential. *J. Chem. Phys.* **2014**, *141*, 174104.
(42) Ehara, M.; Fukuda, R.; Sommerfeld, T. Projected CAP/SAC-CI method with smooth Voronoi potential for calculating resonance states. *J. Comput. Chem.* **2015**, DOI: 10.1002/jcc.24010.
(43) Frisch, M. J.; Trucks, G. W.; Schlegel, H. B.; Scuseria, G. E.; Robb, M. A.; Cheeseman, J. R.; Scalmani, G.; Barone, V.; Mennucci, B.; Petersson, G. A.; et al. *Gaussian Development Version, Revision H.20+;* Wallingford, CT, 2010.
(44) Dunning, T. H. Gaussian-basis sets for use in correlated molecular calculations. 1. The atoms boron through neon and hydrogen. *J. Chem. Phys.* **1989**, *90*, 1007−1023.
(45) Wilson, A. K.; vanMourik, T.; Dunning, T. H. Gaussian basis sets for use in correlated molecular calculations 0.6. Sextuple zeta correlation consistent basis sets for boron through neon. *J. Mol. Struct.: THEOCHEM* **1996**, *388*, 339−349.
(46) Muth-Bohm, J.; Becker, A.; Faisal, F. H. M. Suppressed molecular ionization for a class of diatomics in intense femtosecond laser fields. *Phys. Rev. Lett.* **2000**, *85*, 2280−2283.
(47) Kjeldsen, T. K.; Madsen, L. B. Strong-field ionization of diatomic molecules and companion atoms: Strong-field approximation and tunneling theory including nuclear motion. *Phys. Rev. A: At., Mol., Opt. Phys.* **2005**, *71*, 023411.

DOI: 10.1021/acs.jpca.5b06481
J. Phys. Chem. A 2015, 119, 10212−10220